Electronic Supplementary Material (ESI) for Physical Chemistry Chemical Physics.


**Supplementary Information**

# Rates and equilibrium constants of the ligand-induced conformational transition of an HCN ion channel protein domain determined by DEER spectroscopy

Alberto Collauto[1], Hannah DeBerg[2,3], Royi Kaufmann[1], William N. Zagotta[3], Stefan Stoll[2,3,*] and Daniella Goldfarb[1,*]

[1]Department of Chemical Physics, Weizmann Institute of Science, Rehovot, 76100, Israel
[2]Department of Chemistry, University of Washington, Seattle, WA 98195, USA
[2]Department of Physiology and Biophysics, University of Washington, Seattle, WA 98195, USA

## Contents

1. Analysis of DEER data ....2
2. Data analysis using Tikhonov regularization ....3
3. Global DEER analysis of all DEER data ....4
4. Estimation of the equilibrium constants from DEER data ....4
5. Analysis of the results from the traces obtained under equilibrium conditions....6
6. Modeling of the time-dependent results ....7
7. The μRFQ setup .... 11
8. Calibration of the time scale of the μRFQ setup .... 12
9. The effect of the DEER evolution time. .... 15
10. Orientation selection DEER measurements.... 16

# 1. Analysis of DEER data

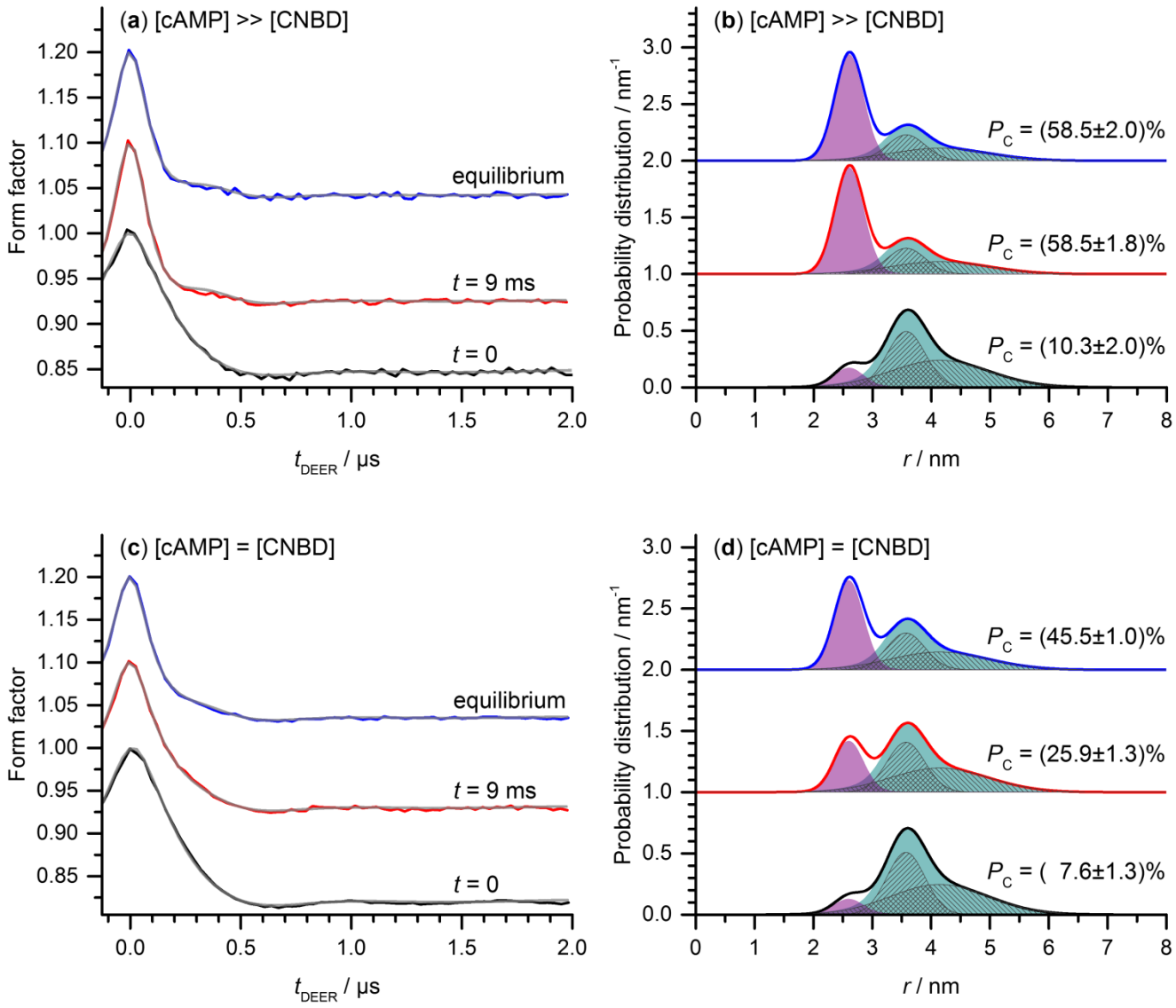


**Figure S1.** (a) Analysis of the DEER experiments by Gaussian fitting of the experimental traces obtained under excess of cAMP ([CNBD] = 22 µM and [cAMP] = 3.8 mM; *t* = 0: [cAMP] = 0). The shaded areas in the plot of the probability distribution highlight the components assigned to the closed conformation (purple) and to the open conformation (cyan). The open conformation is described as a sum of two Gaussian components indicated in black with diagonal fill patterns. (b) Gaussian fitting of the experimental traces obtained with stoichiometric cAMP ([CNDB] = 46 µM and [cAMP] = 46 µM; *t* = 0: [cAMP] = 0). The color coding is the same as in (a). The fractional population of the closed conformation is given next to each trace.

## 2. Data analysis using Tikhonov regularization

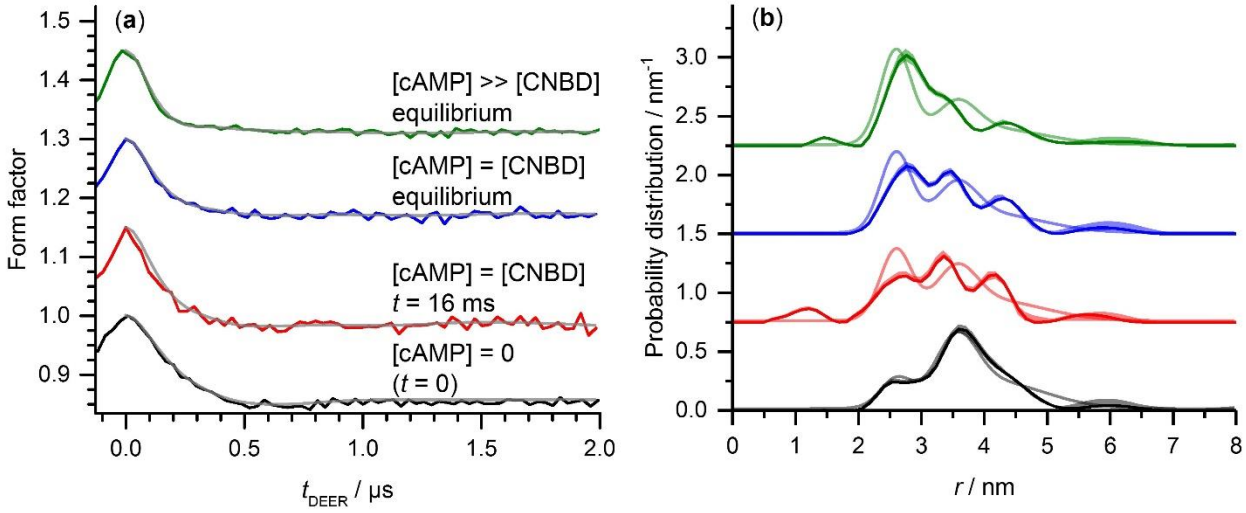


**Figure S2.** Tikhonov regularization ($\alpha$ = 100) analysis of the experimental DEER traces obtained without cAMP (black traces), using a stoichiometric amount of cAMP (red and blue traces), and upon incubation with 5 mM cAMP (116-fold molar excess, green traces); for all the samples [CNBD] = 43 µM. (a) DEER data after background subtraction along with the fit obtained with the Tikhonov regularization-derived distance distributions shown in (b). The shaded areas in (b) show the result of the validation of the background correction, where the starting point was varied between 0.3 and 1.3 µs. These are compared with the distance distributions obtained with the global fit with three Gaussians (light color), shown in Fig.4c.

# 3. Global DEER analysis of all DEER data

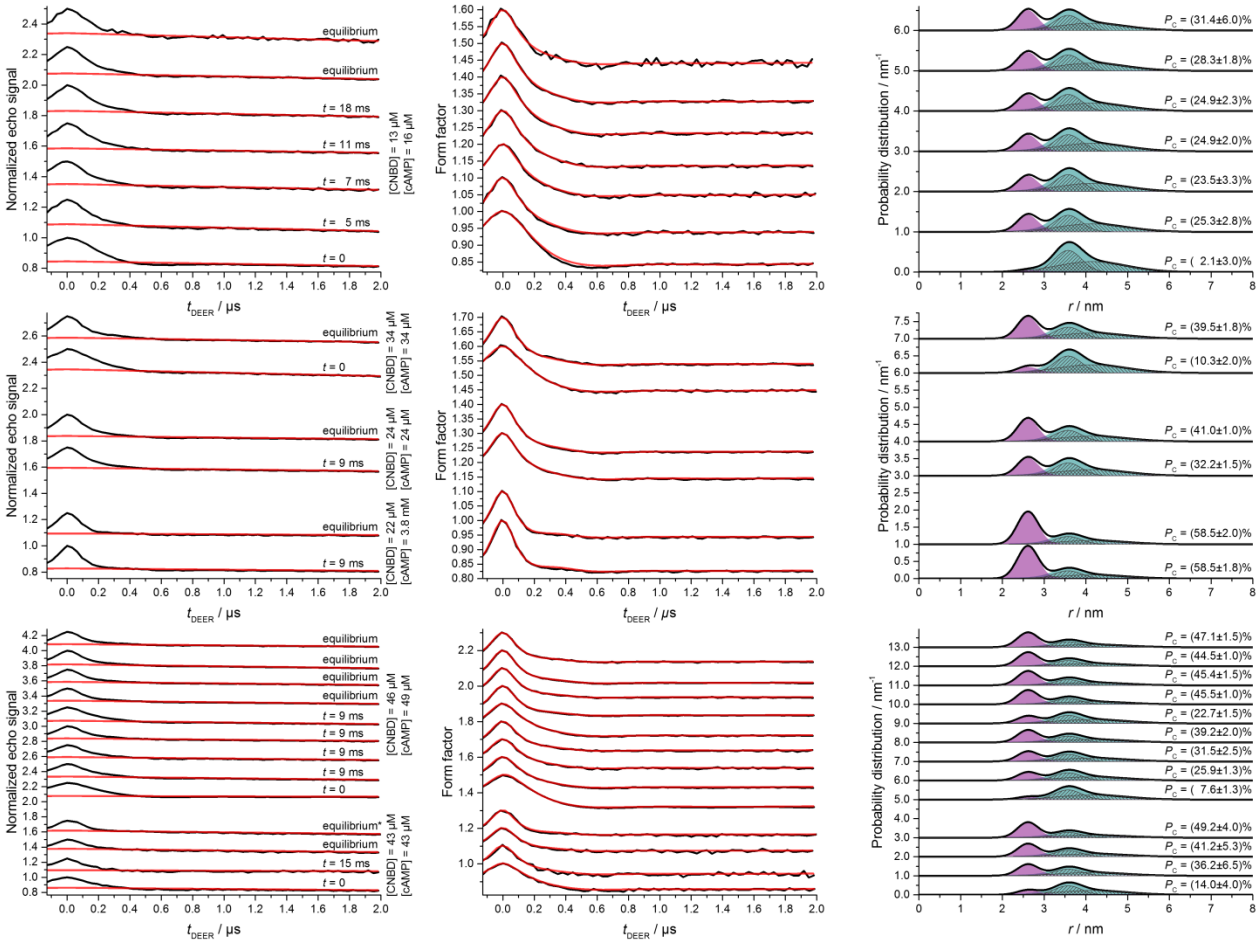


**Figure S3.** Gaussian fitting of all the experimental traces; the shaded areas in the plot of the probability distribution highlight the components assigned to the closed conformation (purple) and to the open conformation (cyan); for [CNDB] = 43 µM, the trace "Equilibrium*" was obtained upon incubation with 5 mM cAMP (116-fold molar excess) rather than with a nearly equimolar ratio between the two components. The traces are grouped as presented in Fig. 5. Left column: Primary DEER data with the background fit. Middle column: Data in the left column after background removal, and fit with the multi-Gaussian distance distributions shown in the right column.

# 4. Estimation of the equilibrium constants from DEER data

Within the four-state model, we can derive an expression for the equilibrium value of the close-to-open ratio $\rho = \frac{[\mathrm{AC}]+[\mathrm{BC}]}{[\mathrm{AO}]+[\mathrm{BO}]}$, which we can then use to analyze the population results from the DEER data using least-squares fitting. First, the conformational equilibrium constants can be used to transform the equation for $K_\mathrm{D}$ to give

$$K_\mathrm{D} = \frac{[\mathrm{AO}](1+K_\mathrm{A})}{[\mathrm{BO}](1+K_\mathrm{B})}[\mathrm{L}] \quad \longrightarrow \quad \frac{[\mathrm{BO}]}{[\mathrm{AO}]} = \frac{(1+K_\mathrm{A})}{(1+K_\mathrm{B})}\frac{[\mathrm{L}]}{K_\mathrm{D}} \tag{S1}$$

Eliminating $[\mathrm{AC}]$ and $[\mathrm{BC}]$ in the expression for $\rho_{\mathrm{eq}}$ ($\rho$ under equilibrium conditions) using the definitions of $K_{\mathrm{A}}$ and $K_{\mathrm{B}}$, and inserting the expression for $[\mathrm{BO}]/[\mathrm{AO}]$, we get

$$\rho_{\mathrm{eq}} = \frac{K_{\mathrm{A}}[\mathrm{AO}]+K_{\mathrm{B}}[\mathrm{BO}]}{[\mathrm{AO}]+[\mathrm{BO}]} = \frac{K_{\mathrm{A}}+K_{\mathrm{B}}[\mathrm{BO}]/[\mathrm{AO}]}{1+[\mathrm{BO}]/[\mathrm{AO}]} = \frac{K_{\mathrm{A}}+K_{\mathrm{B}}\frac{(1+K_{\mathrm{A}})[\mathrm{L}]}{(1+K_{\mathrm{B}})K_{\mathrm{D}}}}{1+\frac{(1+K_{\mathrm{A}})[\mathrm{L}]}{(1+K_{\mathrm{B}})K_{\mathrm{D}}}} = \frac{K_{\mathrm{A}}K_{\mathrm{D}}(1+K_{\mathrm{B}})+K_{\mathrm{B}}(1+K_{\mathrm{A}})[\mathrm{L}]}{K_{\mathrm{D}}(1+K_{\mathrm{B}})+(1+K_{\mathrm{A}})[\mathrm{L}]} \tag{S2}$$

This general expression simplifies for two special cases. First, the case of no ligand. Then, $[\mathrm{L}] = 0$, and we get simply

$$\rho_{\mathrm{eq},0} = K_{\mathrm{A}} \qquad (c_{\mathrm{L}} = 0) \tag{S4}$$

In the case of excess ligand, we have $c_{\mathrm{L}} \gg c_{\mathrm{P}}$, and $[\mathrm{L}] \approx c_{\mathrm{L}}$. This leads to

$$\rho_{\mathrm{eq,xc}} \approx \frac{K_{\mathrm{A}}K_{\mathrm{D}}(1+K_{\mathrm{B}})+K_{\mathrm{B}}(1+K_{\mathrm{A}})c_{\mathrm{L}}}{K_{\mathrm{D}}(1+K_{\mathrm{B}})+(1+K_{\mathrm{A}})c_{\mathrm{L}}} \qquad (c_{\mathrm{L}} \gg c_{\mathrm{P}}) \tag{S5}$$

As expected, this depends on the dissociation constant and on the total ligand concentration. If we additionally have $c_{\mathrm{L}} \gg K_{\mathrm{D}}$, the second terms in the enumerator and the denominator dominate. To understand how this condition affects $\rho_{\mathrm{eq}}$, we first write $\rho_{\mathrm{eq}}$ in terms of $q = K_{\mathrm{D}}/c_{\mathrm{L}}$ and then expand in a power series of $q$ around 0:

$$\rho_{\mathrm{eq}} = K_{\mathrm{B}} + (K_{\mathrm{A}} - K_{\mathrm{B}})\frac{1+K_{\mathrm{B}}}{1+K_{\mathrm{A}}} \cdot q + O(q^2) \tag{S6}$$

This shows that $\rho_{\mathrm{eq}}$ approaches $K_{\mathrm{B}}$ for $c_{\mathrm{L}} \gg K_{\mathrm{D}}$ as long as the prefactor of the linear term is not large. For our case of $K_{\mathrm{B}} > 1 > K_{\mathrm{A}} > 0$, this can be approximated by the requirement that $c_{\mathrm{L}}/K_{\mathrm{D}} \gg K_{\mathrm{B}}^2$, a quite interesting finding. Also, the power series shows that using $K_{\mathrm{B}} \approx \rho_{\mathrm{eq,xc}}$ will overestimate $K_{\mathrm{B}}$.

Continuing with the general expression, the mass balance equation for the ligand gives $[\mathrm{BO}] + [\mathrm{BC}] = c_{\mathrm{L}} - [\mathrm{L}]$, which can be used to replace the denominator of $K_{\mathrm{D}}$. Subtracting the two mass balance equations yields $[L] = c_{\mathrm{L}} - c_{\mathrm{P}} + [\mathrm{AO}] + [\mathrm{AC}]$, which rearranges to $[\mathrm{AO}] + [\mathrm{AC}] = [\mathrm{L}] + c_{\mathrm{P}} - c_{\mathrm{L}} = [\mathrm{L}] + \Delta c$ (with the abbreviation $\Delta c = c_{\mathrm{P}} - c_{\mathrm{L}}$) and can be used to replace the enumerator of $K_{\mathrm{D}}$. Together, this gives

$$K_{\mathrm{D}} = \frac{[\mathrm{L}]+\Delta c}{c_{\mathrm{L}}-[\mathrm{L}]}[\mathrm{L}] \tag{S7}$$

This is a quadratic equation in $[\mathrm{L}]$, $[\mathrm{L}]^2 + [\mathrm{L}](K_{\mathrm{D}} + \Delta c) - K_{\mathrm{D}}c_{\mathrm{L}} = 0$, with the one non-negative solution

$$[\mathrm{L}] = \frac{1}{2}\left(\sqrt{(K_{\mathrm{D}} + \Delta c)^2 + 4K_{\mathrm{D}}c_{\mathrm{L}}} - (K_{\mathrm{D}} + \Delta c)\right) \tag{S8}$$

(The other one is always negative.) This expression for $[\mathrm{L}]$ can now be inserted into the expression for $\rho_{\mathrm{eq}}$, which can be used to determine $K_{\mathrm{D}}$ from datasets of $\rho_{\mathrm{eq}}$, $K_{\mathrm{A}}$, $K_{\mathrm{B}}$, $c_{\mathrm{P}}$ and $c_{\mathrm{L}}$ under general conditions.

## 5. Analysis of the results from the traces obtained under equilibrium conditions

From the expression for $\rho_{eq}$ obtained above under equilibrium conditions, estimates of $K_{\mathrm{A}}$, $K_{\mathrm{B}}$ and $K_{\mathrm{D}}$ can be obtained by fixing $K_{\mathrm{A}}$ and $K_{\mathrm{B}}$ to the values of $\rho_{eq}$ without ligand ($\rho_{\mathrm{eq},0}$) and with excess ligand ($\rho_{\mathrm{eq,xc}}$), respectively. The results of this calculation of $K_{\mathrm{A}}$ and $K_{\mathrm{B}}$ for all samples are listed in Table S1. With these results, $K_{\mathrm{D}}$ can be calculated by inverting the equations shown above. The results are listed in Table S2. As an alternative, it is possible to use values of $K_{\mathrm{D}}$ reported in the literature, fix either $K_{\mathrm{A}}$ or $K_{\mathrm{B}}$ to the corresponding limiting value of $\rho_{eq}$ and obtain the remaining equilibrium constant by inverting the equation for $\rho_{\mathrm{eq}}$:

$$K_{\mathrm{B}} = \frac{\rho_{\mathrm{eq}}K_{\mathrm{D}} + \rho_{\mathrm{eq}}[\mathrm{L}](1+K_{\mathrm{A}}) - K_{\mathrm{A}}K_{\mathrm{D}}}{-\rho_{\mathrm{eq}}K_{\mathrm{D}} + [\mathrm{L}](1+K_{\mathrm{A}}) + K_{\mathrm{A}}K_{\mathrm{D}}} \qquad \text{(S9)}$$

or

$$K_{\mathrm{A}} = \frac{\rho_{\mathrm{eq}}K_{\mathrm{D}}(1+K_{\mathrm{B}}) + (\rho_{\mathrm{eq}} - K_{\mathrm{B}})[\mathrm{L}]}{K_{\mathrm{D}}(1+K_{\mathrm{B}}) + (K_{\mathrm{B}} - \rho_{\mathrm{eq}})[\mathrm{L}]} \qquad \text{(S10)}$$

respectively, where $[\mathrm{L}]$ is given by Eq (S8).

**Table S1**. Estimation of $K_A$ and $K_B$ from the measurements of $\rho_{eq}$ without ligand and with excess ligand, respectively. The uncertainties of the $\rho_{eq}$ values are determined by propagation of the uncertainties in the populations resulting from the GLADD analysis.

| [CNBD] | [cAMP] | $\rho_{eq}$ |
|---|---|---|
| 13.1 µM | 0.0 µM | 0.022±0.031 |
| 33.9 µM | 0.0 µM | 0.115±0.022 |
| 42.5 µM | 0.0 µM | 0.16±0.05 |
| 46.0 µM | 0.0 µM | 0.082±0.014 |
| | **<$K_A$>** | **0.086±0.011** |

| [CNBD] | [cAMP] | $\rho_{eq}$ |
|---|---|---|
| 21.9 µM | 3.8 mM | 1.41±0.08 |
| 42.5 µM | 5.0 mM | 0.97±0.11 |
| | **<$K_B$>** | **1.25±0.07** |

**Table S2.** Estimation of the $K_D$, $K_A$ and $K_B$ values from measurements of $\rho_{eq}$ under equilibrium conditions in the presence of ligand and with known ($K_A$, $K_B$), ($K_A$, $K_D$) or ($K_B$, $K_D$) values, respectively. The uncertainties of $\rho_{eq}$ are determined by propagation of the uncertainties in the populations resulting from the GLADD analysis.

| | | | **$K_A$ = 0.086±0.011**<br>**$K_B$ = 1.25±0.07** | | **$K_A$ = 0.086±0.011**<br>**$K_D$ = (8.0±1.0) µM[4]** | | **$K_B$ = 1.25±0.07**<br>**$K_D$ = (8.0±1.0) µM[4]** | |
|---|---|---|---|---|---|---|---|---|
| [CNBD] | [cAMP] | $\rho_{eq}$ | $K_D$ | | $K_B$ | | $K_A$ | |
| 13.1 µM | 16.3 µM | 0.399±0.025 | (13.9±2.3) µM | | 0.86±0.10 | | -0.03±0.04 | |
| 23.6 µM | 23.6 µM | 0.696±0.021 | (3.1±0.6) µM | | 2.01±0.23 | | 0.29±0.05 | |
| 33.9 µM | 33.9 µM | 0.653±0.035 | (5.8±1.4) µM | | 1.44±0.15 | | 0.16±0.06 | |
| 42.5 µM | 42.5 µM | 0.70±0.11 | (5.5±3.6) µM | | 1.45±0.36 | | 0.17±0.15 | |
| 46.0 µM | 48.5 µM | 0.830±0.014 | (3.3±0.8) µM | | 1.69±0.11 | | 0.31±0.06 | |
| 21.9 µM | 3.8 mM | 1.41±0.08 | | | 1.41±0.08 | | | |
| 42.5 µM | 5.0 mM | 0.97±0.11 | | | 0.97±0.11 | | | |
| | | | **<$K_D$>** | **(3.9±0.4) µM** | **<$K_B$>** | **1.30±0.05** | **<$K_A$>** | **0.153±0.024** |
| | | | **<$K_{DO}$>** | **(8.1±1.0) µM** | **<$K_{DO}$>** | **(16.9±2.2) µM** | **<$K_{DO}$>** | **(15.6±2.0) µM** |

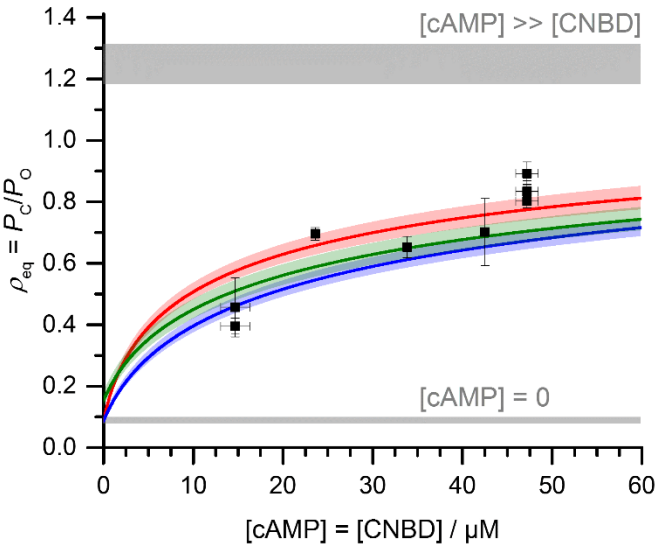


**Figure S4.** Plot of $\rho_{eq}$ as a function of the protein/ligand concentration for samples prepared under equimolar or nearly equimolar conditions. Vertical error bars are determined by propagation of the uncertainties in the populations resulting from the GLADD analysis. Horizontal error bars are drawn for samples prepared under nearly equimolar conditions and reflect the difference between the protein and the ligand concentrations. The lower and upper grey shaded areas show the limiting values of $\rho_{eq}$ obtained with excess ligand and without ligand, respectively (see Table S1). The colored lines represent the modeling of the experimental data performed according to the four-state model described in the main text, where the constants $K_A$ and $K_B$ and $K_D$ were set to the values shown in Table S2 (red trace: $K_A$ = 0.086 ± 0.011, $K_B$ = 1.25 ± 0.07, $K_D$ = (3.9 ± 0.4) µM; blue trace: $K_A$ = 0.086 ± 0.011 , $K_B$ = 1.30 ± 0.05, $K_D$ = (8.0 ± 1.0) µM; green trace: $K_A$ = 0.153 ± 0.024, $K_B$ = 1.25 ± 0.07, $K_D$ = (8.0 ± 1.0) µM). The colored shaded areas, displaying the uncertainty on the calculated $\rho_{eq}$ in terms of +/- one standard deviation, were obtained by propagation of the uncertainties on $K_A$, $K_B$, $K_D$.

## 6. Modeling of the time-dependent results

The kinetics of the interconversion between the four states of the model, namely AO (apo/open), AC (apo/closed), BO (bound/open), and BC (bound/closed), is modelled using the following set of rate equations

$$\begin{cases} \frac{\mathrm{d[AO]}}{\mathrm{d}t} = +k_{\mathrm{Ab}}[\mathrm{AC}] + k_{\mathrm{off}}[\mathrm{BO}] - k_{\mathrm{Af}}[\mathrm{AO}] - k_{\mathrm{on}}[\mathrm{AO}][\mathrm{L}] \\ \frac{\mathrm{d[AC]}}{\mathrm{d}t} = +k_{\mathrm{Af}}[\mathrm{AO}] - k_{\mathrm{Ab}}[\mathrm{AC}] \\ \frac{\mathrm{d[BO]}}{\mathrm{d}t} = +k_{\mathrm{Bb}}[\mathrm{BC}] + k_{\mathrm{on}}[\mathrm{AO}][\mathrm{L}] - k_{\mathrm{Bf}}[\mathrm{BO}] - k_{\mathrm{off}}[\mathrm{BO}] \\ \frac{\mathrm{d[BC]}}{\mathrm{d}t} = +k_{\mathrm{Bf}}[\mathrm{BO}] - k_{\mathrm{Bb}}[\mathrm{BC}] \\ \frac{\mathrm{d[L]}}{\mathrm{d}t} = +k_{\mathrm{off}}[\mathrm{BO}] - k_{\mathrm{on}}[\mathrm{AO}][\mathrm{L}] \end{cases} \quad \text{(S11)}$$

At equilibrium, the forward reaction rates $k_{\mathrm{Af}}$, $k_{\mathrm{Bf}}$ and the backward reaction rates $k_{\mathrm{Ab}}$, $k_{\mathrm{Bb}}$ for the conformational equilibria as well as the on- and off-rates $k_{\mathrm{on}}$ and $k_{\mathrm{off}}$ of the binding equilibrium are related by

$$k_{\mathrm{Af}}/k_{\mathrm{Ab}} = K_{\mathrm{A}}, \qquad k_{\mathrm{Bf}}/k_{\mathrm{Bb}} = K_{\mathrm{B}}, \qquad k_{\mathrm{off}}/k_{\mathrm{on}} = K_{\mathrm{DO}} \tag{S12}$$

For the initial condition, the total concentration of the protein in its apo state, $[\mathrm{AC}] + [\mathrm{AO}]$, is equal to the total protein concentration, $c_{\mathrm{P}}$, with the ratio between [AC] and [AO] being equal to $K_{\mathrm{A}}$, whereas the concentration of free ligand, [L], is equal to the total ligand concentration, $c_{\mathrm{L}}$. The bound states BO and BC are initially unpopulated.

$$\begin{cases} [\mathrm{AO}](0) = c_{\mathrm{P}}/(1 + K_{\mathrm{A}}) \\ [\mathrm{AC}](0) = c_{\mathrm{P}}K_{\mathrm{A}}/(1 + K_{\mathrm{A}}) \\ [\mathrm{BO}](0) = 0 \\ [\mathrm{BC}](0) = 0 \\ [\mathrm{L}](0) = c_{\mathrm{L}} \end{cases} \tag{S12}$$

For each of the concentrations for which time-resolved experiments were performed (given in Table S3), numerical solutions of the system of coupled differential equations were evaluated for a grid of 26×26×26 $(k_{\mathrm{Af}}, k_{\mathrm{Bf}}, k_{\mathrm{off}})$ values, where the value of each rate constant was varied logarithmically between $10^{-2.5}$ $\mathrm{ms}^{-1}$ and $10^{+2.5}$ $\mathrm{ms}^{-1}$. The corresponding values of the backward rate constants were calculated using the $K_{\mathrm{A}}$, $K_{\mathrm{B}}$ and $K_{\mathrm{DO}}$ values that were determined from the analysis of the DEER traces obtained under equilibrium conditions (see previous Section).

**Table S3**. Summary of the RFQ measurements made.

| $c_{\mathrm{P}}$ | $c_{\mathrm{L}}$ | Samples |
|---|---|---|
| 1. 13.1 µM | 16.3 µM | *t* = 0, *t* = 4.6 ms, *t* = 7.2 ms, *t* = 11.2 ms, *t* = 17.5 ms, equilibrium (2 repeats) |
| 2. 23.6 µM | 23.6 µM | *t* = 9.2 ms, equilibrium |
| 3. 42.5 µM | 42.5 µM | *t* = 0, *t* = 15.6 ms, equilibrium |
| 4. 46.0 µM | 48.4 µM | *t* = 0, *t* = 9.2 ms (4 repeats), equilibrium (4 repeats) |
| 5. 21.9 µM | 3.8 mM | *t* = 9.2 ms, equilibrium |

Among all the parameter sets for which the simulations were performed, the ones giving modeled kinetic traces close to the experimental data were selected by sorting the modeled kinetic traces according to the goodness of fit. For this purpose, for each of the conditions listed in Table S3, the uncertainty-weighted residual sum of squares (RSS) was evaluated as

$$RSS_w(k_{\mathrm{Af}}, k_{\mathrm{Bf}}, k_{\mathrm{off}}; c_{P,i}, c_{L,i}) = \frac{\sum_j \left( \left[ \rho^{\mathrm{exp}}(c_{\mathrm{P},i}, c_{\mathrm{L},i}, t_j) - \rho^{\mathrm{calc}}(c_{\mathrm{P},i}, c_{\mathrm{L},i}, t_j, k_{\mathrm{Af}}, k_{\mathrm{Bf}}, k_{\mathrm{off}}) \right]^2 \cdot w_{i,j} \right)}{\sum_j w_{i,j}} \tag{S13}$$

where *i* corresponds to the experiment number in Table S3 and *j* is the index to the particular time point $t_j$, and

$$w_{i,j} = \frac{1}{\sigma_\rho^2(c_{\mathrm{P},i}, c_{\mathrm{L},j})} \tag{S14}$$

where $\sigma_\rho^2$ represents the variance of $\rho$.

Plots of sections of the $RSS_w$ hypersurfaces revealed a substantial independence of the goodness of fit with respect to the $k_{\mathrm{Af}}$ value for the samples prepared under an equimolar or nearly equimolar ratio between the concentrations of cAMP and CNBD (entries 1-4 in Table S3). The effect of $k_{\mathrm{Af}}$ is, however, more pronounced for the sample prepared under excess cAMP (entry 5 in Table S3), and in this case the comparison between the experimental and the calculated traces allows us to set a lower limit for $k_{\mathrm{Af}}$, which is 0.032 $ms^{-1}$ or 0.100 $ms^{-1}$ depending on the choice of the values of the equilibrium constants (see Table S4).

**Table S4.** Values of the rate constants giving a reasonable agreement between the experimental and the modeled kinetic traces.

| | **$K_A$ = 0.086±0.011**<br>**$K_B$ = 1.25±0.07**<br>**$K_D$ = (3.9 ± 0.4) µM**<br>**$K_{DO}$ = (8.1 ± 1.0) µM** | **$K_A$ = 0.086±0.011**<br>**$K_B$ = 1.30 ± 0.05**<br>**$K_D$ = (8.0±1.0) µM[4]**<br>**$K_{DO}$ = (16.9 ± 2.2) µM** | **$K_A$ = 0.153 ± 0.024**<br>**$K_B$ = 1.25±0.07**<br>**$K_D$ = (8.0±1.0) µM[4]**<br>**$K_{DO}$ = (15.6 ± 2.0) µM** |
|---|---|---|---|
| $k_{\mathrm{Af}}$ | > 0.032 $ms^{-1}$ | > 0.032 $ms^{-1}$ | > 0.100 $ms^{-1}$ |
| $k_{\mathrm{Ab}}$ | > 0.37 $ms^{-1}$ | > 0.37 $ms^{-1}$ | > 0.65 $ms^{-1}$ |
| $k_{\mathrm{Bf}}$ | > 2.5 $ms^{-1}$ | > 2.5 $ms^{-1}$ | > 2.5 $ms^{-1}$ |
| $k_{\mathrm{Bb}}$ | > 2.0 $ms^{-1}$ | > 1.9 $ms^{-1}$ | > 2.0 $ms^{-1}$ |
| $k_{\mathrm{off}}$ | (0.023 – 0.054) $ms^{-1}$ | (0.074 – 0.126) $ms^{-1}$ | (0.047 – 0.091) $ms^{-1}$ |
| $k_{\mathrm{on}}$ | (2.9 – 6.6) $mM^{-1}$ $ms^{-1}$ | (4.4 – 7.4) $mM^{-1}$ $ms^{-1}$ | (3.0 – 5.8) $mM^{-1}$ $ms^{-1}$ |

Time traces calculated for $k_{\mathrm{Af}}$ exceeding the aforementioned values no longer affect the data; this allows sections of the $RSS_w$ hypersurfaces taken at a large enough $k_{\mathrm{Af}}$ value (in the specific instance $k_{\mathrm{Af}}$ = 1.0 $ms^{-1}$) to be used in the evaluation of $k_{\mathrm{Bf}}$ and $k_{\mathrm{off}}$, giving a reasonable agreement with the experimental data, thus reducing the complexity of the problem. The results are shown in Fig. S5 and S6.

Inspection of the $RSS_w|_{k_{\mathrm{Af}}=1.0\ \mathrm{ms}^{-1}}$ surfaces reveals the following behavior: for samples prepared under equimolar conditions two ensembles of ($k_{\mathrm{Bf}}$, $k_{\mathrm{off}}$) values could be identified giving a reasonable agreement between the calculated and the experimental traces, corresponding to the rate limiting step being either the ligand binding or the conformational change in the bound state: $k_{\mathrm{Bf}}$ in the range $[k_{\mathrm{Bf,min}}, +\infty)$ and $k_{\mathrm{off}}$ within $[k_{\mathrm{off,min}}, k_{\mathrm{off,max}}]$, or $k_{\mathrm{Bf}}$ within $[k_{\mathrm{Bf,min}}, k_{\mathrm{Bf,max}}]$ and $k_{\mathrm{off}}$ belonging to $[k_{\mathrm{off,min}}, +\infty)$ respectively. However, we know that for the sample prepared under excess cAMP the conformational change already happened within 9.2 ms and that the rate-limiting process is the ligand binding. This in turn restricts the problem of fitting the kinetic traces to finding the minimum $k_{\mathrm{Bf}}$ value and the optimal $k_{\mathrm{off}}$ range with which the experimental data could be satisfactorily reproduced.

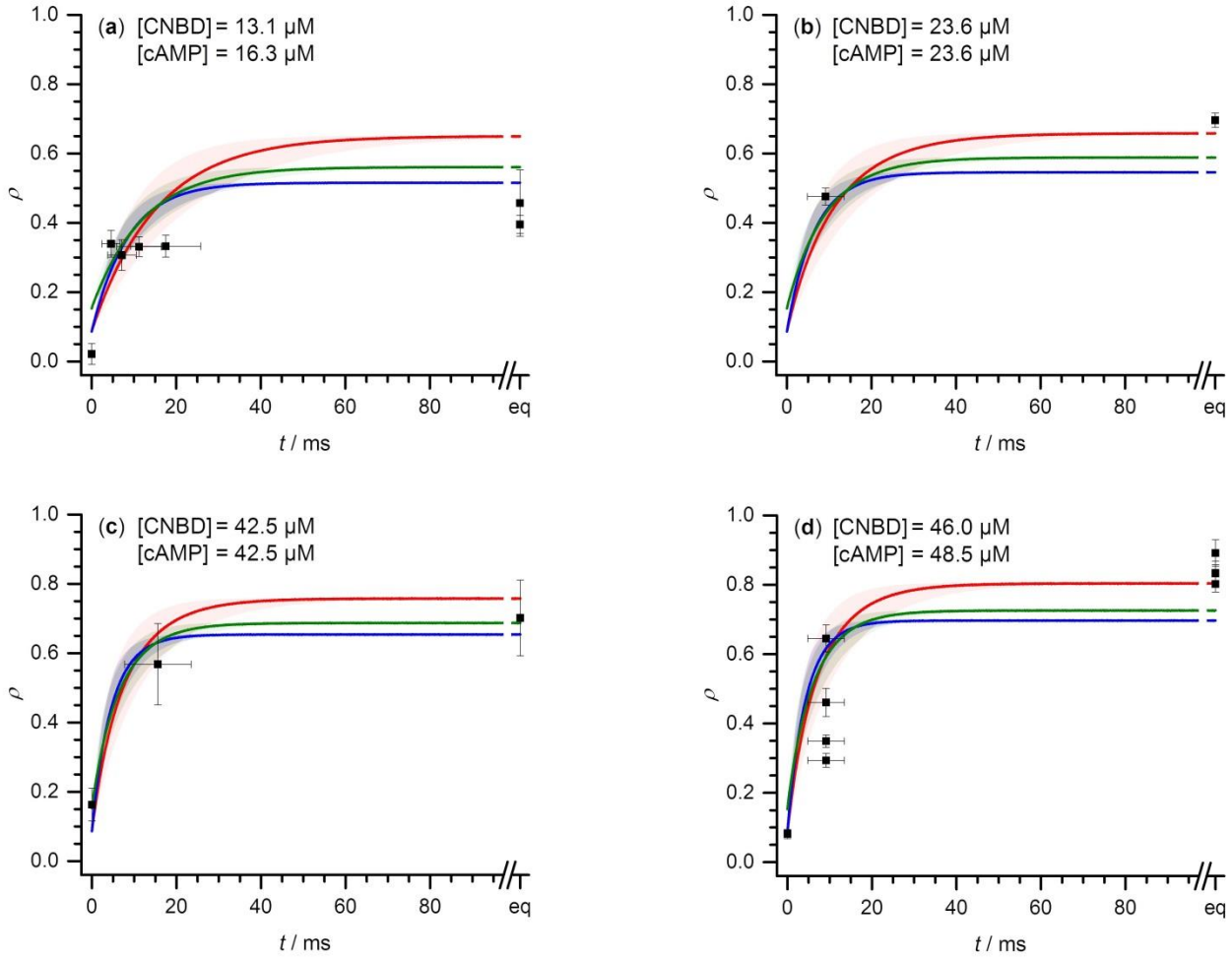


**Figure S5.** Average (solid lines) and envelope (shaded areas) of the model traces calculated using the sets of rate constants displayed in Table S4 for the sets of experiments 1-4 listed in Table S3, corresponding to samples prepared under an equimolar or nearly equimolar ratio between the concentrations of cAMP and CNBD. The color code is related to the choice of the equilibrium constant values $K_A$, $K_B$, $K_D$ and is consistent with the analysis shown in Fig. S4. Black squares: experimental $\rho$ values; the vertical error bars were obtained from propagation of the uncertainties on the populations of the open and closed conformations resulting from the GLADD analysis.

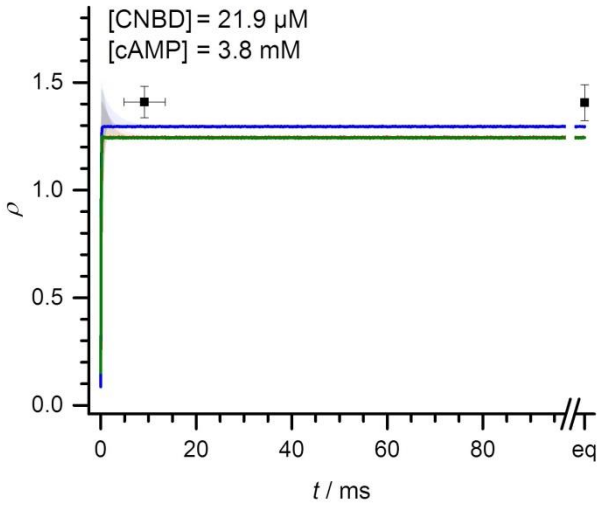


**Figure S6.** Average (solid lines) and envelope (shaded areas) of the model traces calculated using the sets of rate constants displayed in Table S4 for the experiments 5 listed in Table S3, corresponding to the samples prepared under excess cAMP. The color code is related to the choice of the equilibrium constant values KA, KB, KD and is consistent with the analysis shown in Fig. S4. Black squares: experimental $\rho$ values; the vertical error bars were obtained from propagation of the uncertainties on the populations of the open and closed conformations resulting from the GLADD analysis.

## 7. The µRFQ setup

Fig. S7 shows the geometry of the microfluidic mixing structure of our setup and the results of optical profilometry height measurements of the mixing structure. Fig. S8 shows our improved design of the rotating aluminum plate used for quenching and sample collecting. Compared to our original design, the back of the plate has larger surface area, allowing faster cooldown with liquid nitrogen.

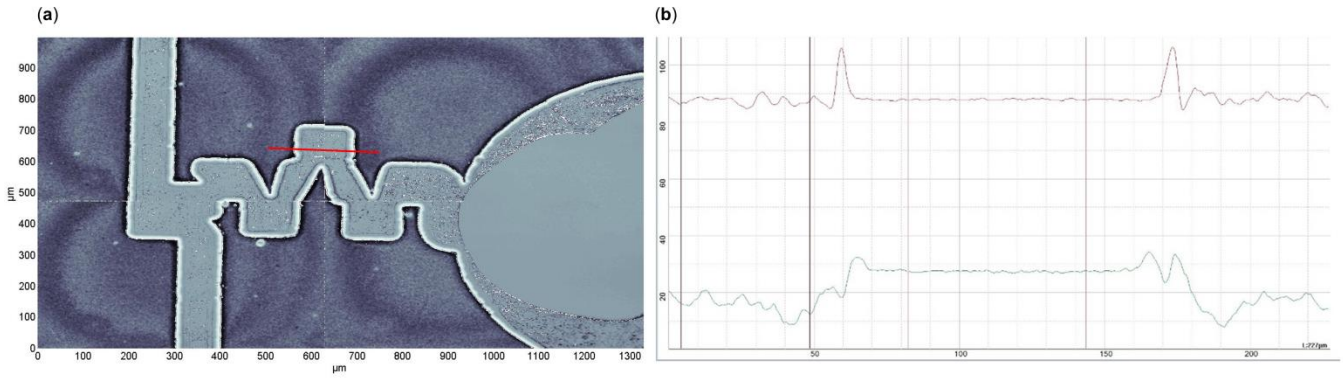


**Figure S7**. The mixing device. (a) Pattern of the passive alcove-based mixer. (b) Determination of the height of the microfluidic channels by optical profilometry. The top trace corresponds to the glass-to-air interface and the lower trace corresponds to the air-to-PDMS interface. The difference between the z-coordinates of the two surfaces, equal to 61 µm along the section highlighted in red in (a), corresponds to the height of the microfluidic channel.

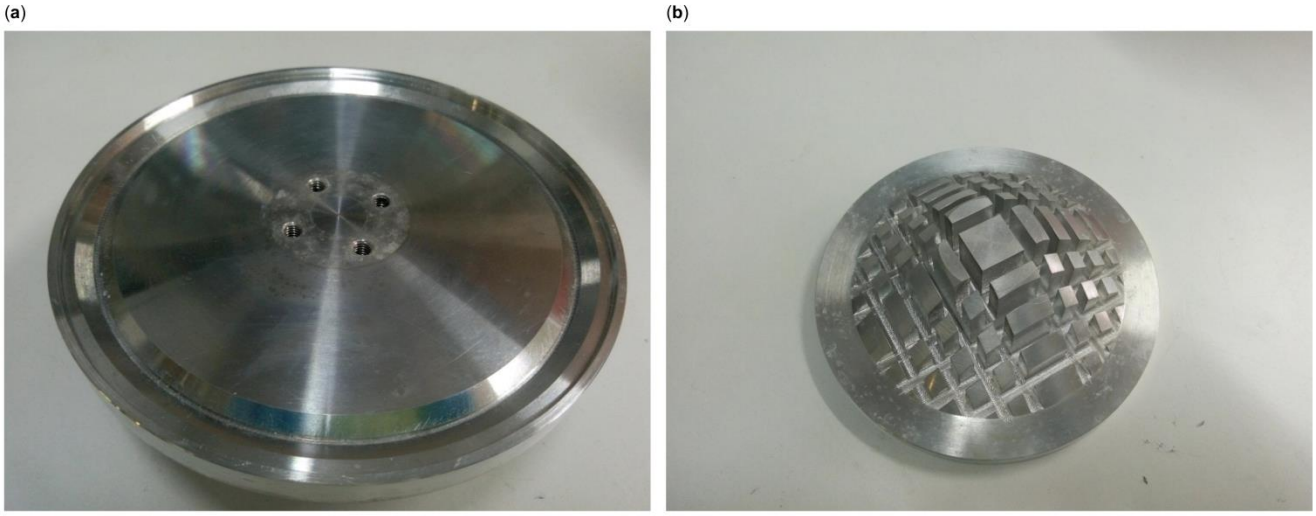


**Figure S8**. The improved collecting aluminum plate. (a) Top view. (b) Bottom view.

## 8. Calibration of the time scale of the μRFQ setup

The calibration of the reaction times for the microfluidic device was performed as previously described[1] using the reduction of TEMPOL to TEMPO by dithionite, with $Mn^{2+}$ as an internal EPR intensity standard. Briefly, two solutions, one containing 500 μM TEMPOL + 1 mM $MnCl_2$ and the other containing 250 mM sodium dithionite + 1 mM $MnCl_2$, both in 100 mM MOPS buffer at pH 7.0, were mixed and quenched using the μRFQ apparatus at various flow rates. After mixing, the initial concentrations are reduced by a factor of two since equal volumes of the two solutions are mixed. An additional sample, corresponding to the endpoint of the reaction and marked in the plots as "equilibrium", was prepared by manually mixing the two solutions in a 1:1 volume ratio and incubating the resulting solution at room temperature for approximately 30 minutes. Echo-detected EPR spectra of the trapped samples (Fig. S9a) were collected using the pulse sequence $\pi/2 - \tau - \pi - \tau -$ echo with $\tau$ = 200 ns, $t_{\pi/2}$ = 22.5 ns and $t_{\pi}$ = 45 ns, where the microwave power was adjusted in order to get $t_{\pi}$ = 25 ns on the high-field hyperfine line of the Mn(II) sextet. The shot repetition time and the scan rate were set to 50 ms and 0.13 mT $s^{-1}$, respectively, and a two-step phase cycle +(+x) - (-x) was applied to the first microwave pulse. All the spectra were normalized to the intensity of the high-field $Mn^{2+}$ hyperfine line.

The intensity of the spectrum at the magnetic field corresponding to the maximum of the nitroxide spectrum after normalization (Fig. S9b) shows an increase of the signal as a function of the pre-mixing volume flow rate $F$, which is proportional to the reciprocal of the reaction time. The intensity of the pre-steady-state nitroxide spectrum, obtained by subtracting the signal of the equilibrium sample, is expected to follow first-order kinetics

$$I_{\mathrm{N-O}}(t) = I_{\mathrm{N-O}}(0) \cdot \mathrm{e}^{-kt} = I_{\mathrm{N-O}}(0) \cdot \mathrm{e}^{-k\left(\frac{V_{\mathrm{eff}}}{2F}\right)} \qquad \text{(S15)}$$

where $V_{\mathrm{eff}}$ is the effective volume of the mixing chamber and $2F$ is the flow rate after mixing.

A semilogarithmic plot of $I_{\mathrm{N-O}}(t)$ versus $\frac{1}{2F}$ (Fig. S10a) yields a slope $b = -kV_{\mathrm{eff}} = (-7.4 \pm 3.4)\ \mu\mathrm{L\ s^{-1}}$. For the reduction reaction of TEMPOL with dithionite, the tabulated value of the second-order rate constant is $k' = (800 \pm 100)\ \mathrm{M^{-1}s^{-1}}$ [2,3], hence for the dithionite concentration used in this experiment the pseudo-first order rate constant *k* is $k = k'[\mathrm{dithionite}] = (100 \pm 12.5)\ \mathrm{s^{-1}}$. From this it follows that the effective volume of the mixing chamber is $V_{\mathrm{eff}} = (74 \pm 35)\ \mathrm{nL}$. This value is close to the one calculated according to the geometry of the device, $V_{\mathrm{geom}} = 92\ \mathrm{nL}$.

A semilogarithmic plot of $I_{\mathrm{N-O}}(t)$ versus $t = \frac{V_{\mathrm{eff}}}{2F}$ is displayed in Fig. S10b and shows the range of reaction times accessible by the microfluidic device. The estimate of the relative uncertainty of the reaction time, resulting from the propagation of the uncertainty on $V_{\mathrm{eff}}$, is 47%.

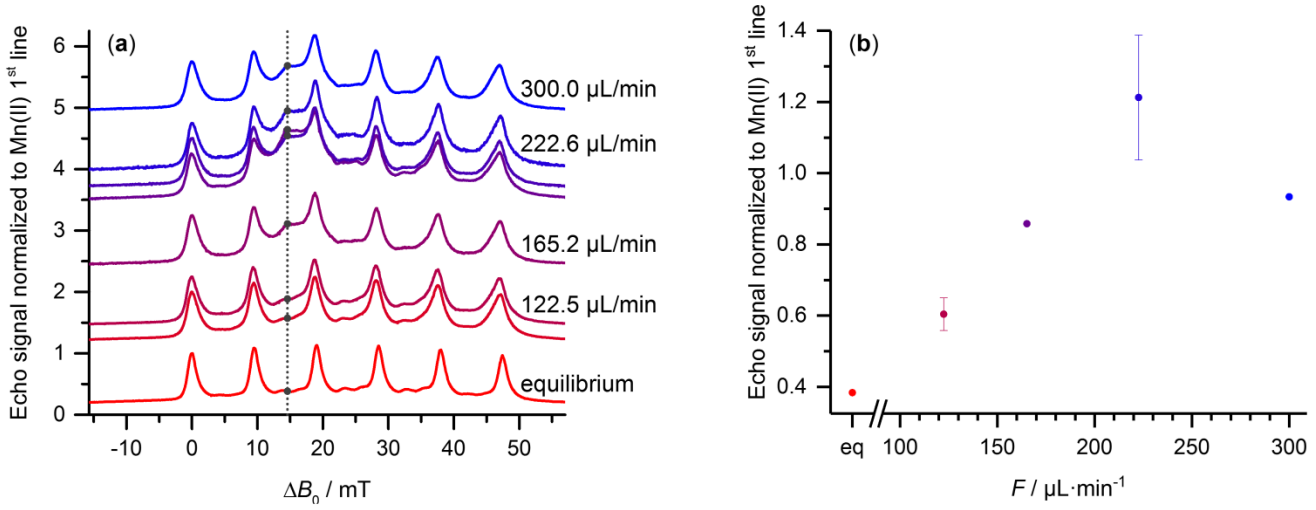


**Figure S9.** (a) Echo-detected EPR spectra of the µRFQ samples of a solution of TEMPOL mixed with dithionite, in the presence of $MnCl_2$ as an internal standard obtained with different flow rates. (b) Plot of the normalized TEMPOL signal (at the position indicated by dots in (a) as a function of pre-mixing flow rate *F*. For more details see text. The error bars were determined from duplicates or triplicates.

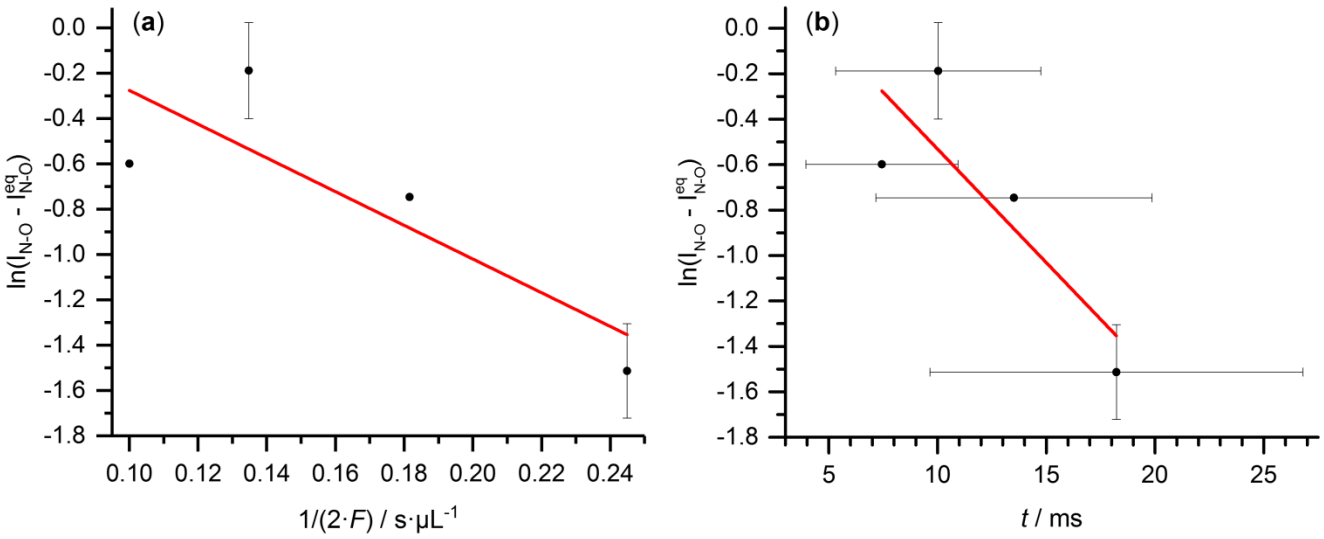


**Figure S10.** Analysis of the data of the time calibration experiment (see text for details). (a) Non-equilibrium signal intensity as a function of reciprocal flow rate. (b) Non-equilibrium signal intensity as a function of time, with time given by $\boldsymbol{t = V_{eff}/2F}$.

## 9. The effect of the DEER evolution time.

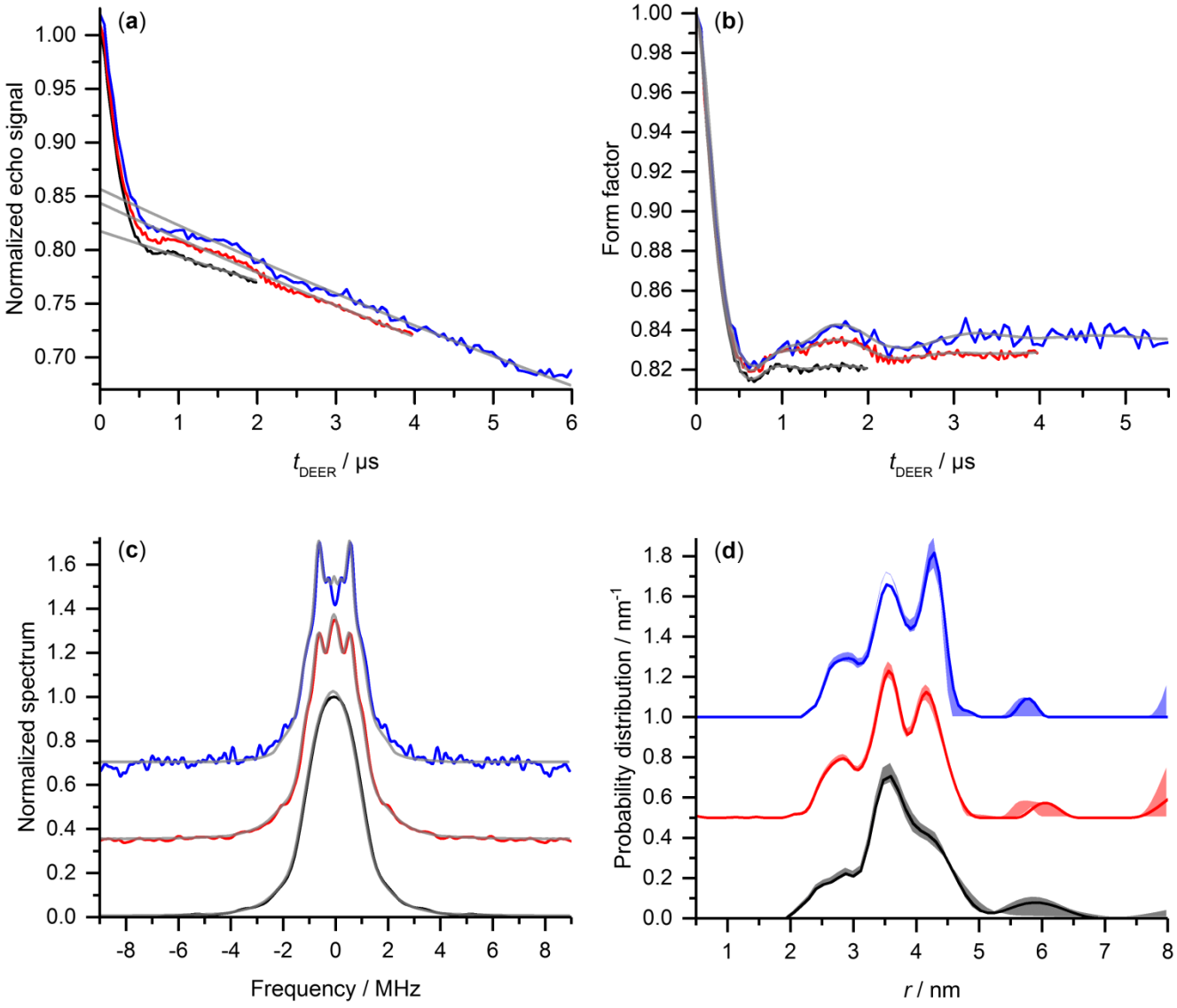


**Figure S11.** DEER traces of HCN2-CNBD without cAMP collected with evolution times of 2 (black), 4 (red) and 6 µs (blue). (a) Primary DEER data (colored) with the background fits (grey). Traces are shifted with respect to each other for clarity. (b) Traces of (a) after background removal, and fits obtained with the distance distributions shown in (d). (c) Fourier transforms of the experimental and fitted traces in (b). (d) Distance distributions fitted using Tikhonov regularization, including error bars; a regularization parameter α = 100 was used for all the traces.

## 10. Orientation selection DEER measurements

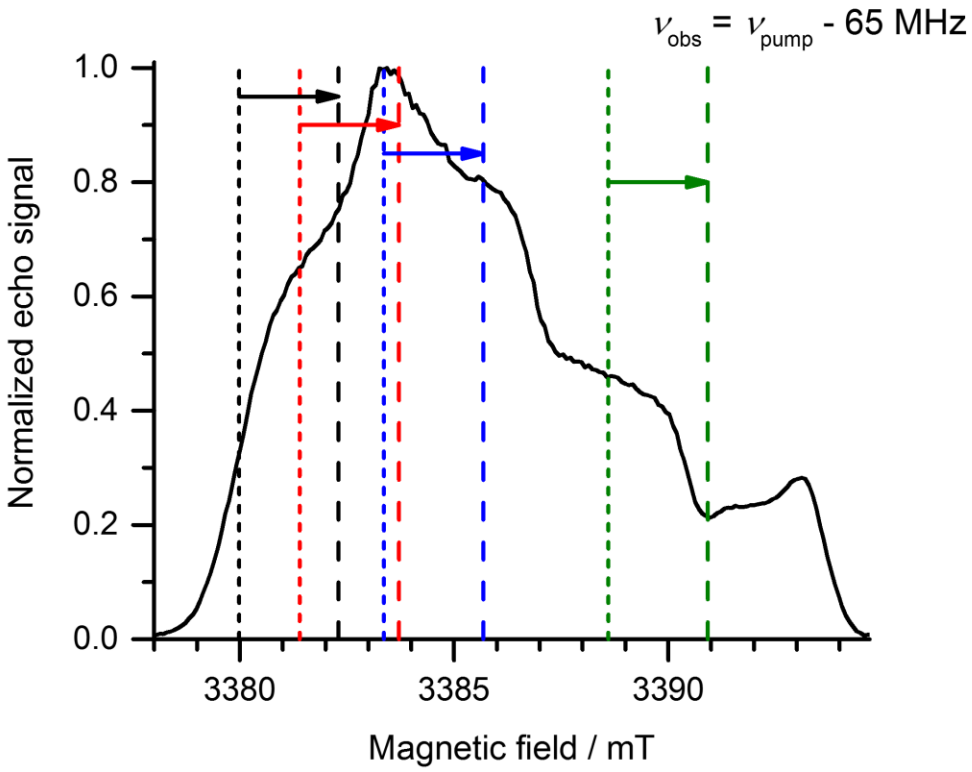


**Figure S12.** Position of pump pulses (short dashes) and observe pulses (long dashes) for the orientation selection DEER experiments. The corresponding DEER data are shown in Fig. S13, with the same color coding. The signal at 3393 mT is due to an impurity.

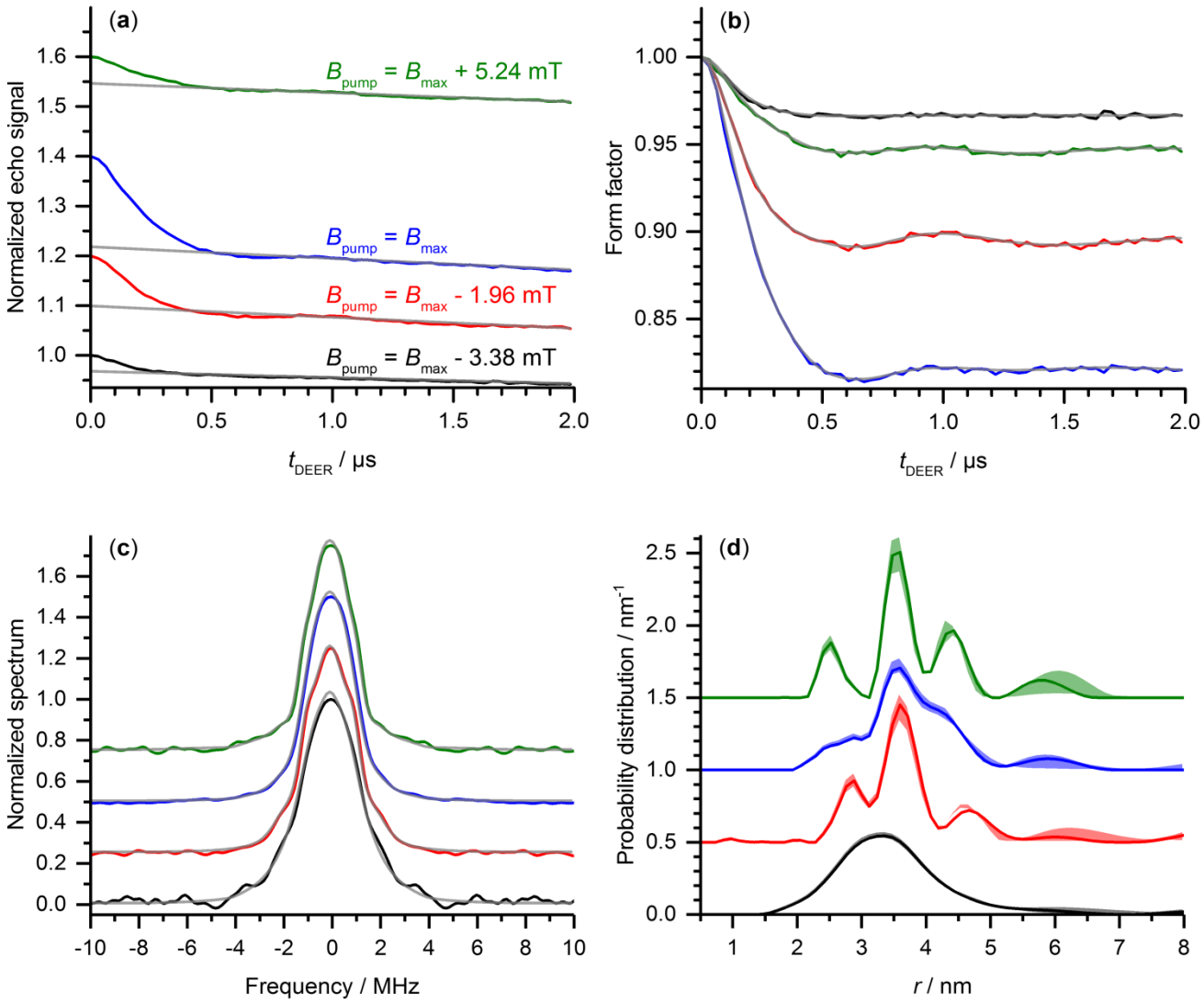


**Figure S13.** DEER data collected with different pump and observe frequencies, as indicated in Fig. S12. (a) Primary DEER data, including fitted background. Traces are shifted with respect to each other for clarity. (b) Traces of (a) after background removal, including Tikhonov-regularized fits. (c) Fourier transforms of traces from (b). (d) Fitted distances distributions obtained by Tikhonov regularization; a regularization parameter α = 100 was used for all the traces except for $B_{pump} = B_{max} - 3.38$ mT (black trace), for which α = 1000 was used. Except for the black trace, all other pulse set up did not exhibit orientation selection.

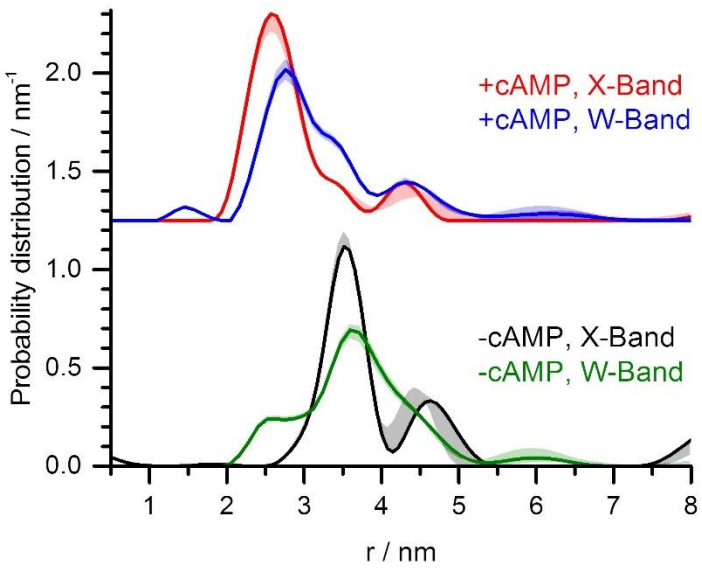


**Figure S14.** Comparison of the X-band and W-band distance distribution of samples without cAMP and with cAMP, as noted on the Figure. The X-band data were taken from reference 5.

## References


1. R. Kaufmann, I. Yadid and D. Goldfarb, *J. Magn. Reson.*, 2013, **230**, 220-226.
2. A. Potapov and D. Goldfarb, *Appl. Magn. Reson.*, 2010, **37**, 845-850.
3. A. Potapov and D. Goldfarb, *Appl. Magn. Reson.*, 2013, **44**, 435-435.
4. H. A. DeBerg, P. S. Brzovic, G. E. Flynn, W. N. Zagotta and S. Stoll, *J. Biol. Chem.*, 2016, **291**, 371-381.
5. M. C. Puljung, H. A. DeBerg, W. N. Zagotta and S. Stoll, *Proc. Natl. Acad. Sci. U S A*, 2014, **111**, 9816-9821.